Prediction of van Hove singularities, excellent thermoelectric performance, and non-trivial topology in monolayer rhenium dichalcogenides

Ina Marie R. Verzola[1], Rovi Angelo B. Villaos[1], Winda Purwitasari[1], Zhi-Quan Huang[1], Chia-Hsiu Hsu[2], Guoqing Chang[2], Hsin Lin[3], and Feng-Chuan Chuang[1,4,5,6,*]

[1]*Department of Physics, National Sun Yat-sen University, Kaohsiung, 80424 Taiwan*

[2]*Division of Physics and Applied Physics, School of Physical and Mathematical Sciences, Nanyang Technological University, 637371 Singapore*

[3]*Institute of Physics, Academia Sinica, Taipei, 115201 Taiwan*

[4]*Physics Division, National Center for Theoretical Sciences, Taipei, 10617 Taiwan*

[5]*Center for Theoretical and Computational Physics, National Sun Yat-sen University, Kaohsiung, 80424 Taiwan*

[6]*Department of Physics, National Tsing Hua University, Hsinchu, 30013 Taiwan*

*Corresponding Author: Feng-Chuan Chuang

Postal Address: 70 Lienhai Rd., Kaohsiung 80424, Taiwan

Telephone: +886-7-5253733

E-mail Address: fchuang@mail.nsysu.edu.tw

Abstract

Two-dimensional (2D) thermoelectric materials are gaining more intense attention with the ever-increasing global demand for energy. Recently, the search for compounds exhibiting excellent thermoelectric and topological characteristics has also attracted research exploration. In this study, a systematic investigation of Re-based transition metal dichalcogenides (TMDs) (ReX_2, X = S, Se, and Te) through first-principles calculations identified the stability and electronic properties of the $1T^{dp}$ (1T double prime), 1T', 1T, and 2H phases for the pristine bulk and monolayer ReX_2. Formation energy and phonon dispersion calculations showed that the bulk and monolayer structures are only stable in the $1T^{dp}$ structure. The calculated bandgaps of bulk under the hybrid functional approach are 1.567 eV, 1.429 eV, and 0.745 eV, while those of the monolayer phases are 1.902 eV, 1.658 eV, and 1.323 eV for ReS_2, $ReSe_2$, and $ReTe_2$, respectively. Moreover, van Hove singularities (vHss) are observed in monolayer ReX_2 suggesting possible superconductivity. Remarkably, the calculated figure of merits (ZT) of bulk and monolayer ReX_2 with values up to 2.30 presents them as excellent materials for thermoelectric (TE) applications since good TE materials have ZT > 0.4. In addition, the effect of one- (1h) and two-sided (2h) hydrogenation on the structural, electronic, magnetic, and topological properties of monolayer ReX_2 were also investigated. Two-sided hydrogenation caused a stable structural phase transition from $1T^{dp}$ to 1T. A ferromagnetic phase transition was also observed upon the two-sided hydrogenation of ReS_2 (2h-ReS_2) and the one-sided hydrogenation of $ReSe_2$ (1h-$ReSe_2$). Finally, one-sided hydrogenation of monolayer $ReSe_2$ and $ReTe_2$ (1h-$ReSe_2$ and 1h-$ReTe_2$) resulted in non-trivial topological phases as confirmed by the calculated Z_2 and Chern topological invariant numbers. Our findings show that the 2D Re-based TMDs exhibit highly tunable properties which have the potential for thermoelectric and spintronics applications.

Keywords: 2D materials, rhenium dichalcogenides, first-principles, van Hove singularities, thermoelectric materials, topological materials

1. Introduction

The escalating global climate change and its environmental effects due to the combustion of fossil fuels are extremely unsettling and are causing immense social and political conflict around the world [1]. One solution to improve the sustainability of electricity is through thermoelectric materials. Thermoelectric (TE) materials are capable of converting heat into electricity or transporting heat-producing cooling using the Seebeck and Peltier effects, respectively [2]. The thermoelectric conversion efficiency of TE materials is determined by the unitless figure of merit (ZT), which is expressed as $ZT = S^2\sigma T/\kappa$, where S, σ, and T are Seebeck coefficient, electrical conductivity, and absolute temperature, while κ is the sum of electronic thermal conductivity (κ_e) and lattice thermal conductivity (κ_l), respectively [3–5]. In order to achieve high TE efficiency, materials with high ZT values are required, in which a large power factor ($S^2\sigma$) and low thermal conductivity at the same time are expected. However, S, σ, and κ are conflictingly correlated with each other [6, 7], making it challenging to obtain materials with high ZT values. New strategies for the development of thermoelectric devices are required to eliminate or at least weaken this dependence among the three parameters.

Interestingly, two-dimensional (2D) materials with a layered structure have garnered considerable attention as efficient thermoelectric materials because of their exceptional advantages in electronic and mechanical properties [8, 9]. Among these 2D materials, a group of compounds known as transition metal dichalcogenides (TMDs) has been gaining a lot of research focus. TMDs are represented by the chemical formula MX_2, where M corresponds to a transition metal and is sandwiched by X atoms corresponding to the chalcogens S, Se, or Te. Studies have shown their versatile and tunable properties, such as indirect-to-direct bandgap

transition, Lifshitz transition [10, 11], and van Hove singularities (vHss) which can be easily manipulated [12]–[14] by tuning their thickness or inducing a strain [11–16]. Additionally, recent studies have shown that the functionalization of TMDs significantly alters and manipulates their electronic, magnetic, and topological properties [10, 11, 15–21]. In fact, 2D TMDs have been studied for their great potential as thermoelectric materials due to their relatively low thermal conductivity and high electrical conductivity [8, 22–24].

Among the emerging TMDs is the rhenium dichalcogenides (ReX_2) which is a new family of 2D TMD semiconductors as it has been successfully fabricated recently [25–27], thus requiring further investigation. It was found that ReX_2 crystallizes in a distorted 1T structure ($1T^{dp}$) due to the charge decoupling from an extra valence electron of rhenium atoms [25–31]. Recent studies about ReX_2 showed that it displayed a monolayer-like electronic structure in the bulk phase [29], as well as pronounced anisotropy as observed in its optical properties [26–31]. The aforementioned characteristics of ReX_2 substantiate its strong potential for next-generation technologies.

On the other hand, in order to be used in device applications, 2D materials must be grown or placed on a suitable substrate. One method that can be used to emulate the effects of substrates is chemical adsorption, particularly hydrogenation [32]. Hydrogenation can be considered as a simplified electron-filling model which is used to adjust the influence of the environment on the electronic structure of the thin film [18, 33–35]. Some studies have shown that the band topology and bandgap of the thin film change significantly after hydrogenation, and the effect of structural changes caused by different functional groups can be achieved by the effect of strain [36]. In addition, several studies on the functionalization of ReX_2 reported structural phase transition and dynamical stability as well as tuned physical and chemical properties [36, 37]. Moreover, a

recent study demonstrated the non-trivial topological phases of ReX_2 in 1T structure upon one-sided hydrogen adsorption and halogen substitution [17]. Despite the recent studies, no work has been done on the hydrogenation and possible topological phases of the experimentally synthesized $1T^{dp}$ structure of ReX_2. Non-trivial materials are attracting intense interest as they offer new possibilities for energy-efficient device applications [38–43]. Among the non-trivial materials are the 2D topological insulators (2D TIs) which are also known as quantum spin Hall (QSH) insulators [40, 44, 45], topological superconductors [29], topological crystalline insulators (TCIs) [46, 47], and quantum anomalous Hall (QAH) insulators [42, 44, 45]. The significance of these developments is the discovery of the quantum Hall effect which gave way to the realization of the topological nature of the electronic structures and the dissipationless spin-transport around the edges of a 2D insulator under a strong magnetic field [48–50].

The purpose of this study is to investigate the structural, electronic, thermoelectric, magnetic, and topological properties of ReX_2 using first-principles calculation. This paper reports on the stability comparison for different existing TMD structures, specifically $1T^{dp}$, 1T', 1T, and 2H to probe the most stable structure of ReX_2. Additionally, this paper investigates property changes in the bandgap size, a direct-to-indirect bandgap transition, and an enhancement of superconductivity due to dimensionality changes of ReX_2 from bulk to monolayer. This paper also studies the thermoelectric properties of bulk and monolayer ReX_2 in terms of the ZT figure of merits. Finally, it demonstrates the effect of one- and two-sided hydrogenation on the structural, electronic, magnetic, and topological characteristics of ReX_2 monolayers.

2. Computational Methods

The Vienna Ab-initio Simulation Package (VASP) [51, 52] was used to perform first-principles calculations within the density functional theory framework [53] with the projected augmented wave (PAW) [54, 55] in the Perdew-Burke-Ernzerhof (PBE) [56] under the generalized gradient approximations (GGA) exchange-correlation functional. The van der Waal (vdW) correction rev-vdW-DF2 functional [57] was used to estimate the experimental lattice parameters. Approximately, a 15.0 Å vacuum was set along the z-direction of the monolayer materials to prevent interactions of the repeated layers. The plane wave cut-off energy was set to 400 eV. All crystal structure relaxations were conducted until the residual force acting on each atom is less than 0.01 eV/Å. Additionally, the requirement for self-consistent calculation convergence was set at 10^{-6} eV. The Γ-centered Monkhorst-Pack [48] grid of 18×18×6(1) for 2H, 18×18×9(1) for 1T, 18×9×18(1) for 1T', and 18×18×18(1) for $1T^{dp}$ phases in bulk(monolayer) were used to model the first Brillouin zone. Additionally, the Heyd-Scuseria-Ernzerhof hybrid functional (HSE06) [58–60] through a reduced Γ-centered Monkhorst-Pack grid of 6×6×6(1) for $1T^{dp}$ bulk(monolayer) was further implemented to correct the electronic band and thermal transport properties. The phonon dispersion calculations were performed using the Phonopy [61] software.

For hydrogen functionalization, hydrogen atoms were added to the chalcogen of the relaxed pristine structures to create both the one- and two-sided hydrogenated ReX_2. After hydrogen adsorption, relaxation of the atomic structure and lattice constants were performed. The abbreviations "0h", "1h", and "2h" were used to label the pristine structure, one-, and two-sided hydrogenation cases, respectively.

Three magnetic configurations were examined to investigate the magnetic property: NM for non-magnetic, FM for ferromagnetic, and AFM for antiferromagnetic. Self-consistent calculations were performed for each magnetic structure and their total energies were compared to determine their magnetic property. In this regard, a material for which the energy difference is less than 1 meV between NM and FM (AFM) and the magnetic moment of the individual atom is less than 0.100 μB in FM and AFM configurations can be regarded as NM. However, for materials with magnetic moments equal to or greater than 0.100 μB, the magnetic moment of each metal atom will be further inspected to confirm whether it is in FM or AFM configuration. The calculations also included spin-polarization and spin-orbit coupling (SOC). The Z2Pack [62, 63] was used to calculate the Z_2 number for NM materials and the Chern number for magnetic configurations to predict the topological phases.

The theoretical approach to calculating the thermoelectric properties of the ReX_2 materials was split into two stages. The first stage computes the electronic thermal properties under HSE06 through semi-classical Boltzmann transport equation (BTE) and relaxation time approximation (RTA) methods for electrons as implemented in the BoltzTraP2 code [64, 65] using a constant relaxation time of $\tau = 10^{-14}\, s$ for thermal and electrical conductivities. The relaxation time value $\tau = 10^{-14}\, s$ is commonly used in semiconductors and its validity has previously been tested and found to be a reasonably good approximation. We assume that the relaxation time is constant and independent of temperature and doping in this case [23, 66]. This calculation gives information about S, σ, and κ_e. Meanwhile, the second stage estimates κ_l through the linearized phonon Boltzmann transport equation (LBTE) method with the inclusion of non-analytical corrections (NAC) to consider long-range interactions via the Phono3py code [67]. As implemented in Phono3py, the phonon relaxation time is assumed by the phonon

lifetime [68, 69]. The second-order force constants for harmonic phonons and the third-order force constants for anharmonic phonons were calculated using the finite-displacement method using a 4×4×1 supercell, a cutoff pair distance of 3 Å, and a q-mesh grid of 12×12×1. We have tested that the supercell size of 4×4×1, cutoff pair distance of 3 Å, and q-mesh grid size of 12×12×1 have reached the convergence needed for the lattice thermal conductivity.

3. Results and Discussion

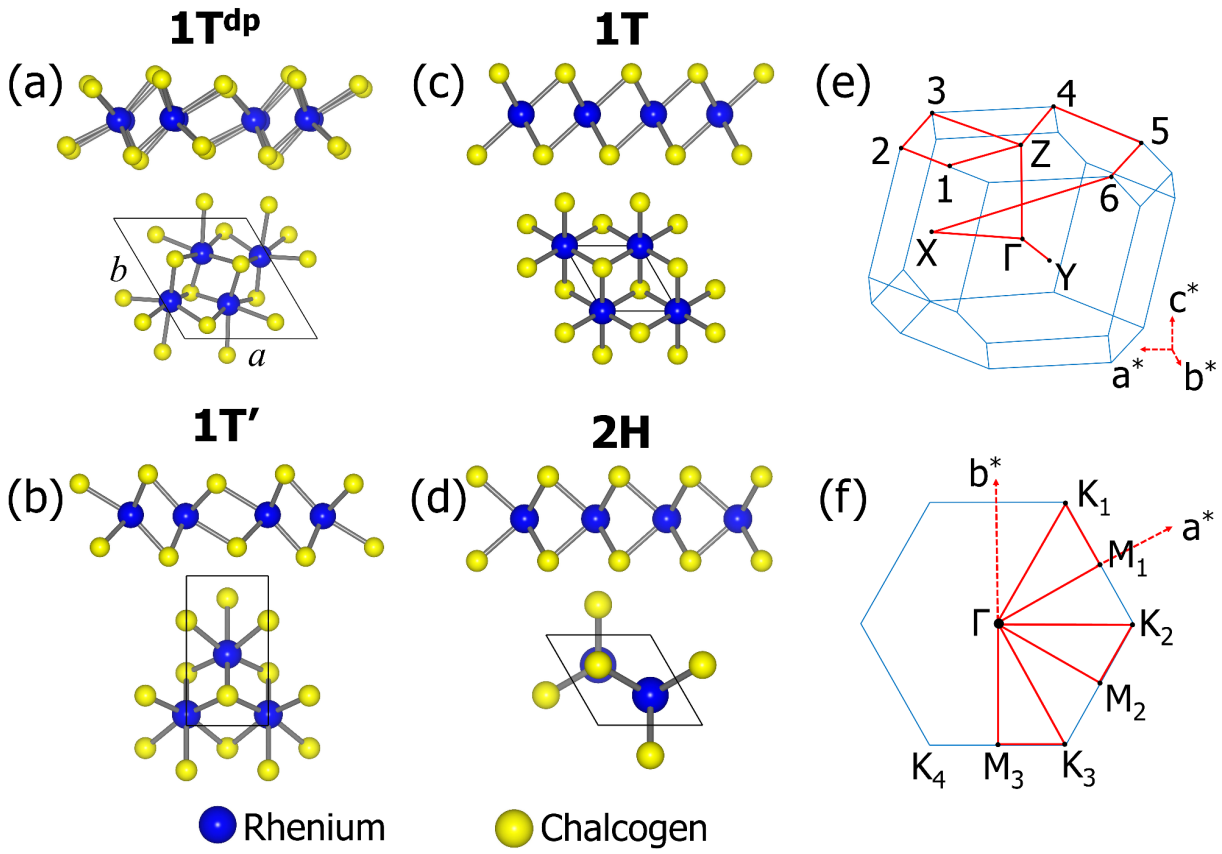

Figure 1. Perspective views of the different structural phases of pristine bulk ReX_2 in side-view and top-view for (a) $1T^{dp}$, (b) 1T', (c) 1T, and (d) 2H. The first Brillouin zones of (e) bulk and (f) monolayer $1T^{dp}$ with the high-symmetry points.

3.1 Structural Properties and Stability

In this study, we explored the properties of bulk and monolayer ReX_2 (X = S, Se, or Te). The structures of the ReX_2 materials considered in this study are $1T^{dp}$, 1T', 1T, and 2H phases with their perspective views shown in Figures 1(a)-(d). The 1T phase shown in Figure 1(c) belongs to the $P\bar{3}m1$ space group symmetry and is in octahedral prismatic coordination, while the 2H structure shown in Figure 1(d) exhibits trigonal prismatic coordination belonging to the $P6_3/mmc$ space group symmetry. The 1T structure is a 1×1 unit cell containing one transition metal and two chalcogens. Meanwhile, the $1T^{dp}$ structure in Figure 1(a), belongs to the $P\bar{1}$ space group symmetry. It is presented in a 2×2 supercell relative to the 1T phase to model distortion and contains four transition metals and eight chalcogens in the unit cell. Lastly, the 1T' phase has a 1×2 supercell structure, shown in Figure 1(b), and belongs to the group symmetry of $P2_1/m$. The first Brillouin zone (BZ) of the bulk and monolayer $1T^{dp}$ ReX_2 are also shown in Figure 1(e) and (f), respectively.

The lattice parameters obtained upon geometry optimization using vdW correction on the bulk and monolayer ReX_2 materials, as summarized in Table 1, are in good agreement with the experimental data [70–73].

Table 1. The calculated bandgaps under hybrid functional and lattice parameters of the $1T^{dp}$ ReX_2. The experimental bandgaps and lattice constants from related studies are enclosed in parentheses.

	Bulk			**Monolayer**		
	ReS_2	**$ReSe_2$**	**$ReTe_2$**	**ReS_2**	**$ReSe_2$**	**$ReTe_2$**
E_G (eV)	1.567 (1.550)[25]	1.429 (1.290)[74]	0.745	1.902 (1.600)[25]	1.658 (1.470)[71]	1.323
a **(Å)**	6.362 (6.362)[70]	6.618 (6.602)[70]	6.979 (6.882)[71]	6.376 (6.540)[72]	6.638 (6.570)[73]	7.068
b **(Å)**	6.463 (6.455)[70]	6.743 (6.716)[70]	7.117 (7.520)[71]	6.480 (6.720)[72]	6.763 (7.050)[73]	7.207
c **(Å)**	6.284 (6.401)[70]	6.707 (6.728)[70]	7.212 (8.992)[71]	--	--	--

Based on the calculated formation energies summarized in Table S1, $1T^{dp}$ is the most energetically favorable structure for bulk and monolayer ReX_2. This is consistent with the $1T^{dp}$ structure observed experimentally in bulk ReX_2 which is in triclinic atomic configuration [70, 71, 75].

Furthermore, phonon calculations were performed to confirm the thermodynamic stability of the bulk and monolayer ReX_2. As shown in Figure S2, the phonon spectra for all three materials in the $1T^{dp}$ bulk and monolayer phases exhibit non-imaginary frequencies which satisfy the criteria for thermodynamic stability. In contrast, imaginary frequencies were observed among the 1T', 1T, and 2H structures, as shown in Figure S3-5, respectively, confirming that the $1T^{dp}$ is the only stable structure for Re-based TMDs.

3.2 Electronic Properties and van Hove Singularities

To understand the nature of the electronic properties of ReX_2, we calculated their electronic properties through the HSE06 hybrid functional as the PBE functional is known to underestimate the bandgap. The bandgaps for bulk and monolayer band structures under HSE06 are summarized in Table 1. The HSE06 band structures for bulk and monolayer of $1T^{dp}$ ReX_2 calculated using the high-symmetry directions with the inclusion of spin-orbit coupling (SOC) are shown in Figure S6. For the bulk structures, ReS_2 is an insulator with a direct bandgap of 1.567 eV at the Z point. These values are in the same range as the recent theoretical [75] and experimental [76] studies. Interestingly, we also observed an insulating property in the bulk $ReSe_2$ with a direct bandgap of 1.429 eV at the Z-point. Finally, the HSE06 band structure of bulk $ReTe_2$ is an insulator with an indirect bandgap of 0.745 eV.

For monolayer cases, the band structures and density of states (DOS) of ReX_2 in the $1T^{dp}$ phase are plotted in Figure S6 along with the high-symmetry directions of the first BZ. The HSE06 band structure of monolayer ReS_2 remained insulating with an indirect bandgap of 1.902 eV. Meanwhile, the monolayer $ReSe_2$ has an indirect bandgap of 1.658 eV. Finally, the $ReTe_2$ monolayer has an indirect bandgap of 1.323 eV. As seen in Table 1, the bandgaps for the $1T^{dp}$ ReX_2 increased as the dimension decreased from 3D (bulk) to 2D (monolayer).

Van Hove Singularities (vHss) are a fascinating phenomenon that is known to be crucial in improving superconductivity, ferromagnetism, and anti-ferromagnetism of materials as proven in several experimental and theoretical studies [77–81]. Generally, the systems that exhibit vHss have saddle points in their band dispersion. Additionally, diverging peaks in the density of states (DOS) near the Fermi level indicate many states occupying the same energy level.

A diverging DOS, indicated by magenta arrows, is observed in the monolayer $1T^{dp}$ ReS_2, $ReSe_2$, and $ReTe_2$ as shown on the right side of Figure S6. Upon closer observation of the band structures of the three monolayer phases, $1T^{dp}$ ReS_2 has the highest intensity in the diverging DOS (See Figure 2(a)), thus we will use it as the representative material. As seen in Figure 2(a), a sharp peak in the DOS near the Fermi level correlates to a saddle point in the band structure, which is a distinctive characteristic of vHss. The 2D band contour of monolayer $1T^{dp}$ ReS_2 is shown in Figure 2(b). A saddle point around Γ, highlighted by the white circle, attributes to the diverging DOS. These characteristic features exhibited by this material confirm the presence of vHss near the Fermi level, thus suggesting superconductivity.

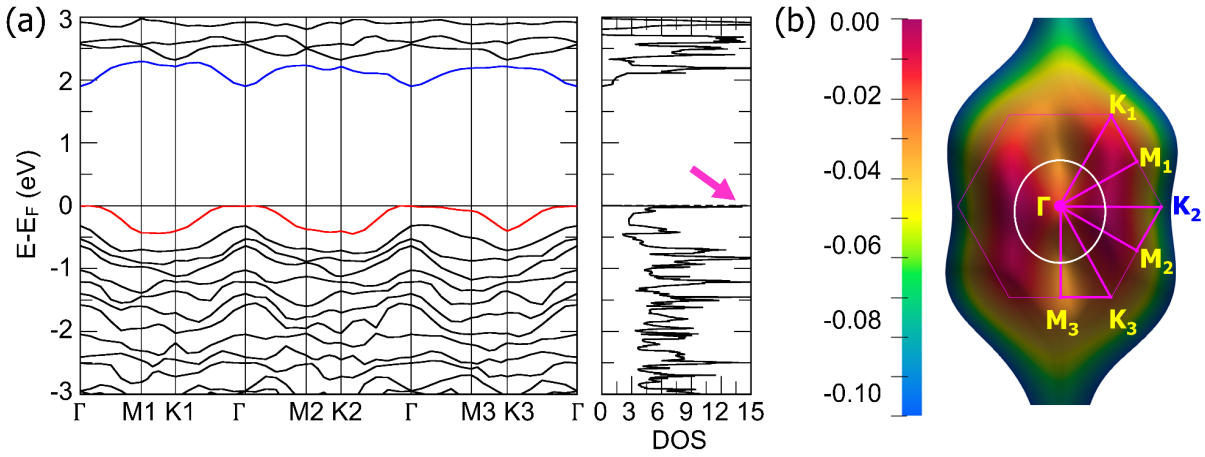

Figure 2. Van Hove singularity in monolayer 1T^{dp} ReS_2. (a) The band structure and DOS were calculated using HSE06 with the inclusion of SOC. (b) The 2D constant-energy band contour with the saddle points highlighted in the white circle was generated using PBE.

3.3 Thermoelectric Properties

Surprisingly, we also found that ReX_2 possesses excellent thermoelectric properties. It is known that the doping level can help improve the thermoelectric properties of materials. The chemical potential (μ) is related to the doping level in the rigid band model [82] wherein a positive μ suggests n-type doping, while a negative μ indicates p-type doping. This relation mainly affects the Seebeck coefficient and conductivity [83]. Here, we present all the thermoelectric parameters with respect to μ and have normalized the Fermi level at 0 eV. The detailed behavior of the thermoelectric properties of the bulk and monolayer ReX_2 are summarized in Figures S15-S19.

To discuss the thermoelectric properties of monolayer ReX_2, we chose $ReTe_2$ as a representative material as it has the best thermoelectric properties among all the studied compounds. The thermoelectric parameters of monolayer $ReTe_2$ are plotted as a function of chemical potential and temperature in Figure 3. Seebeck coefficient S is the most fundamental parameter to understand the response of a material to the applied temperature gradient. The S of monolayer $ReTe_2$ plotted against μ at varying temperatures is shown in Figure 3(a). Surprisingly, S is greatly enhanced in a narrow region around $\mu = 0$, which implies that a significant value of S can already be achieved even with minimal n-type or p-type doping. On the other hand, the electrical conductivities (σ) against the chemical potential with varying temperatures for the monolayer $ReTe_2$ is shown in Figure 3(b). It is observed that σ is higher in the p-type region compared to the n-type at high temperatures.

In general, the power factor (PF) compared to the Seebeck coefficient and electrical conductivity is one of the comprehensive parameters to investigate the thermoelectric performance of a material. The chemical potential dependence of the PF of monolayer $ReTe_2$ is shown in Figure 3(c). It reaches its maximum in the chemical potential interval of [-1.0, 1.0 eV]. High PF values are obtained in the p-type region compared to the n-type. This is because the S and σ of the p-type monolayer $ReTe_2$ are significantly higher compared to its n-type counterpart. However, as the ZT number also depends on the thermal conductivity, the power factor might not reflect the thermoelectric performance directly [84].

To incorporate thermal conductivity, we need both electronic thermal conductivity (κ_e) and lattice thermal conductivity (κ_l). The κ_e is plotted as a function of the chemical potential of monolayer $1T^{dp}$ $ReTe_2$ in Figure 3(d). We found that the κ_e follows the same trend of being flat

near the Fermi level since this area corresponds to the bandgap of the system. Additionally, it is observed that the κ_e increases with temperature. Moving on to κ_l, we have calculated this parameter based on the harmonic phonons and anharmonic force constants. The plot of κ_l with respect to temperature is shown in Figure 3(e) wherein the κ_l decreases as the temperature increases. At high temperatures, low lattice thermal conductivity shows that this material has great potential as a thermoelectric material since many reports conclude that materials with low lattice thermal conductivity have led to exceptionally high ZT numbers [22].

To fully assess the thermoelectric performance of these materials, the ZT figure of merit was calculated. The chemical potential dependence of the ZT number of monolayer $ReTe_2$ is shown in Figure 3(f). Here, the ZT is also maximum in the chemical potential interval of [-1.0, 1.0 eV]. Excellent ZT numbers are obtained in the p-type region compared to the n-type, confirming that this material performs better as a p-type thermoelectric material at 700K.

A more comprehensive summary of the ZT numbers as a function of temperature for the ReX_2 materials is shown in Figure 4 for p-type and n-type thermoelectric materials. Interestingly, both the n-type bulk ReS_2 and $ReSe_2$ have a higher ZT number compared to the monolayer structure. This is due to the higher electrical conductivity of the bulk (See Figures S15(b) and S16(b)), compared to their monolayer counterparts (See Figures S18(b) and S19(b)). In contrast, the ZT number of the bulk $ReTe_2$ structure is lower than its monolayer counterpart at high temperatures. Additionally, it is observed that at 1300K, bulk $ReTe_2$ has the highest ZT number among the bulk materials considered in this study, with a ZT value of 2.10 for both p-type and n-type. Meanwhile, monolayer $ReTe_2$ has superior thermoelectric properties among all materials with ZT values of 2.30 for both p-type and n-type. Furthermore, as observed in Figures 4(a) and (b), the ZT numbers of bulk and monolayer $ReTe_2$ are starting to decrease at 1300K. This

behavior can be attributed to the direct relationship between the bandgap and Seebeck coefficient according to the Goldsmid-Sharp bandgap equation [85]. Among the ReX_2 materials, bulk and monolayer $ReTe_2$ have the smallest bandgaps, as summarized in Table 1. According to the rigid band model, the band structure does not change with temperature, but the Fermi level does [86]. As a result, when the temperature increases, the Fermi level shifts towards the conduction band. Thus, if the material has a relatively small bandgap, a further increase in temperature will cause the material to exhibit metallic behavior. Thus, the Seebeck coefficient and consequently the ZT number will decrease once it reaches a critical temperature. Remarkably, the calculated ZT values confirm that Re-based TMDs exhibit excellent TE performance since the criterion for good TE materials is to have a ZT number above 0.4 [87]. In addition, results reveal that the ZT values of ReX_2 are comparable with the well-known and most studied thermoelectric materials [88].

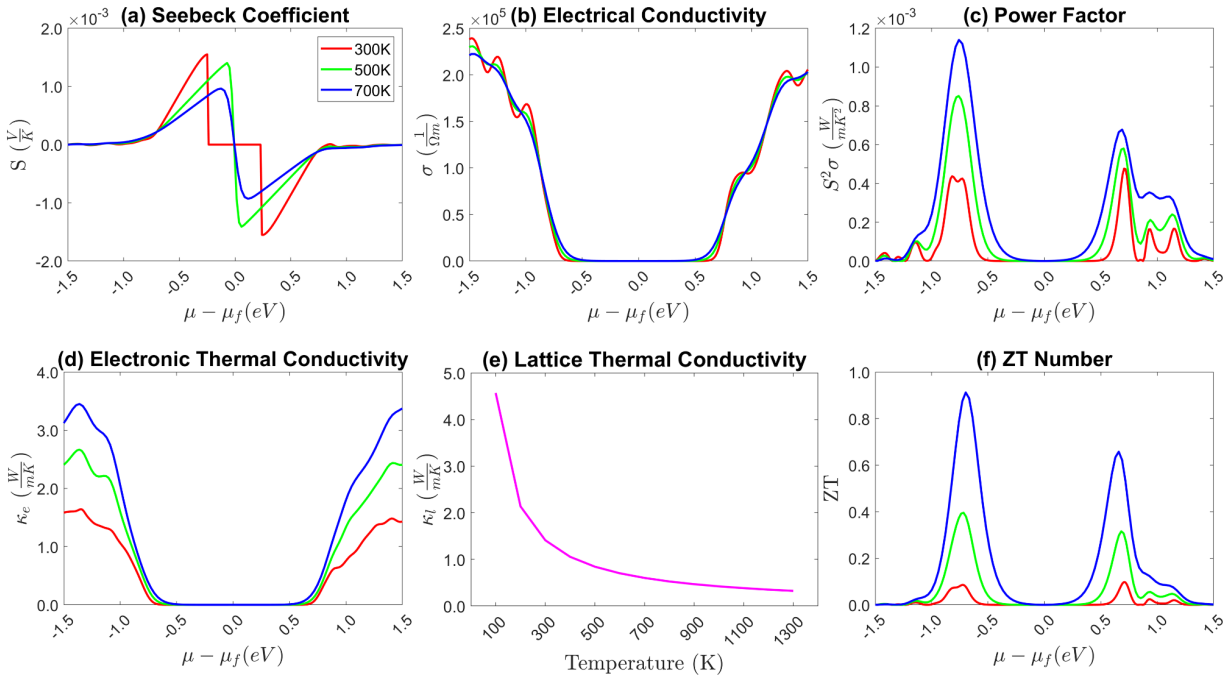

Figure 3. The thermoelectric properties of monolayer $1T^{dp}$ $ReTe_2$. (a) Seebeck coefficient, (b) electrical conductivity, (c) power factor, (d) electronic thermal conductivity, (e) lattice thermal conductivity, and (f) ZT number with respect to temperature and chemical potential.

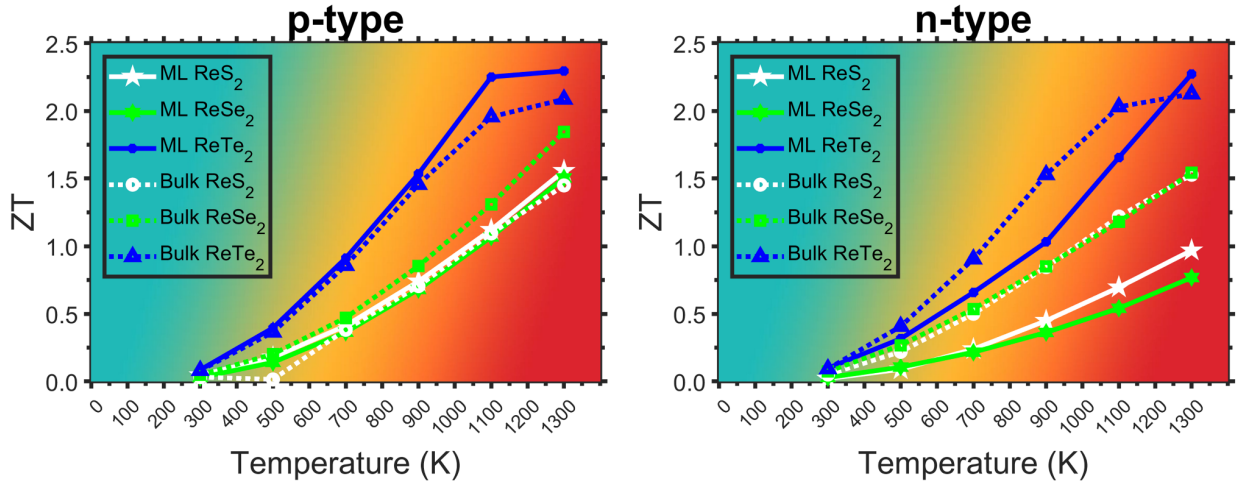

Figure 4. The maximum ZT number of bulk and monolayer (ML) $1T^{dp}$ ReX_2 as a function of temperature for (a) p-type and (b) n-type material.

3.4 Quantum Anomalous Hall Effect in Hydrogenated Monolayer ReX_2

Functionalization of TMDs has been shown in previous theoretical and experimental research to substantially engineer their properties [17, 18, 79]. Specifically, the electronic, magnetic, and topological properties can be modified by functionalization through hydrogenation [18]. With all these interesting physical characteristics found upon hydrogenation of TMDs, it is critical to investigate the induction or manipulation of magnetism, as well as the possibility of topological phases on ReX_2 monolayers.

In this section, we demonstrated the highly tunable properties of ReX_2 through functionalization via hydrogenation. Similar to the pristine case, the structures of the hydrogenated ReX_2 materials considered in this study are $1T^{dp}$, 1T', 1T, and 2H phases with their perspective views shown in Figure S20. Upon one- and two-sided adsorption of hydrogen, we examined the stable phase by observing the formation energy of each material which is summarized in Table S2. The observed stable structural phase transitions upon hydrogenation are then summarized in Table 2. From the previous discussion, the $1T^{dp}$ structure has been identified as the stable phase for the monolayer pristine ReX_2. After one-sided hydrogenation, the stable phase remained $1T^{dp}$. However, a stable phase transition from $1T^{dp}$ to 1T was observed upon two-sided hydrogenation. These transitions in the stable structural phase mainly occurred due to the change of the lattice constants after the adsorption of hydrogen.

Moving on to the magnetic properties of these materials, we summarized the results in Table 2. For the pristine cases, we observed all materials to have NM phases. Upon one-sided

hydrogenation, 1h-ReS_2 and 1h-$ReTe_2$ monolayers retained NM phases while 1h-$ReSe_2$ transitioned to the FM phase. Lastly, two-sided hydrogenation induced an FM phase in ReS_2, while the other two monolayers remained non-magnetic. This significant transition in the magnetic characteristics is due to the change in the total number of electrons and the carrier-mediated double exchange in the system [36].

To have a better understanding of the mechanism that causes the magnetic phase transition, we used 1h-$ReSe_2$ as a representative material for which an NM to FM phase transition occurred due to one-sided hydrogenation. The PBE band structures of 1h-$ReSe_2$ in $1T^{dp}$ are shown in Figure 5. The system received an additional electron after hydrogen adsorption which led to an unequal filling of spin-up and spin-down states and the shifting of the Fermi level. Upon the inclusion of spin-polarization, the separation of spin majority and minority further demonstrated the transition from NM to FM phase due to hydrogen adsorption as shown in Figure 5(c). With the inclusion of SOC in Figure 5(d), we observed further band splitting along the high-symmetry points.

Finally, we determined the topological properties of 1h-ReX_2 ($1T^{dp}$ phase) and 2h-ReX_2 (1T phase) and these results are summarized in Table 2. Remarkably, we found non-trivial topological properties for the functionalized ReX_2 monolayers. For the ferromagnetic 1h-$ReSe_2$, the calculated Chern number is $C = 1$, while the Z_2 number of the non-magnetic 1h-$ReTe_2$ is 1, which confirms their non-trivial topological phases. These results reveal that the hydrogenated monolayer ReX_2 possesses non-trivial topological phases. The effect of hydrogenation on the pristine ReX_2 films causes the Fermi level to shift upward, as shown in Figures S21-22. The addition of one electron to ReX_2 films is responsible for this outcome. Additionally, the

incorporation of SOC, as shown in Figure 5(d), caused the band opening which leads to a non-zero Chern number in 1h-$ReSe_2$, thus confirming a non-trivial phase.

Table 2. Stable structural, magnetic, and topological phases of pristine and hydrogenated ReX_2 monolayers.

ReX_2	Stable Structural Phase			Magnetic Phase			Topological Invariants		
	0h	**1h**	**2h**	**0h**	**1h**	**2h**	**0h**	**1h**	**2h**
S	$1T^{dp}$	$1T^{dp}$	1T	NM	NM	FM	--	$Z_2 = 0$	C = 0
Se	$1T^{dp}$	$1T^{dp}$	1T	NM	FM	NM	--	C = 1	M
Te	$1T^{dp}$	$1T^{dp}$	1T	NM	NM	NM	--	$Z_2 = 1$	M

The Z_2 number $Z_2 = 0$ indicates the trivial phase while $Z_2 = 1$ denotes the non-trivial phase of the non-magnetic materials. On the other hand, the Chern number C = 0 indicates the trivial phase and $C \neq 0$ denotes the non-trivial phase for the ferromagnetic materials. Metallic systems are denoted as M since Z_2 and C invariants do not apply to metals.

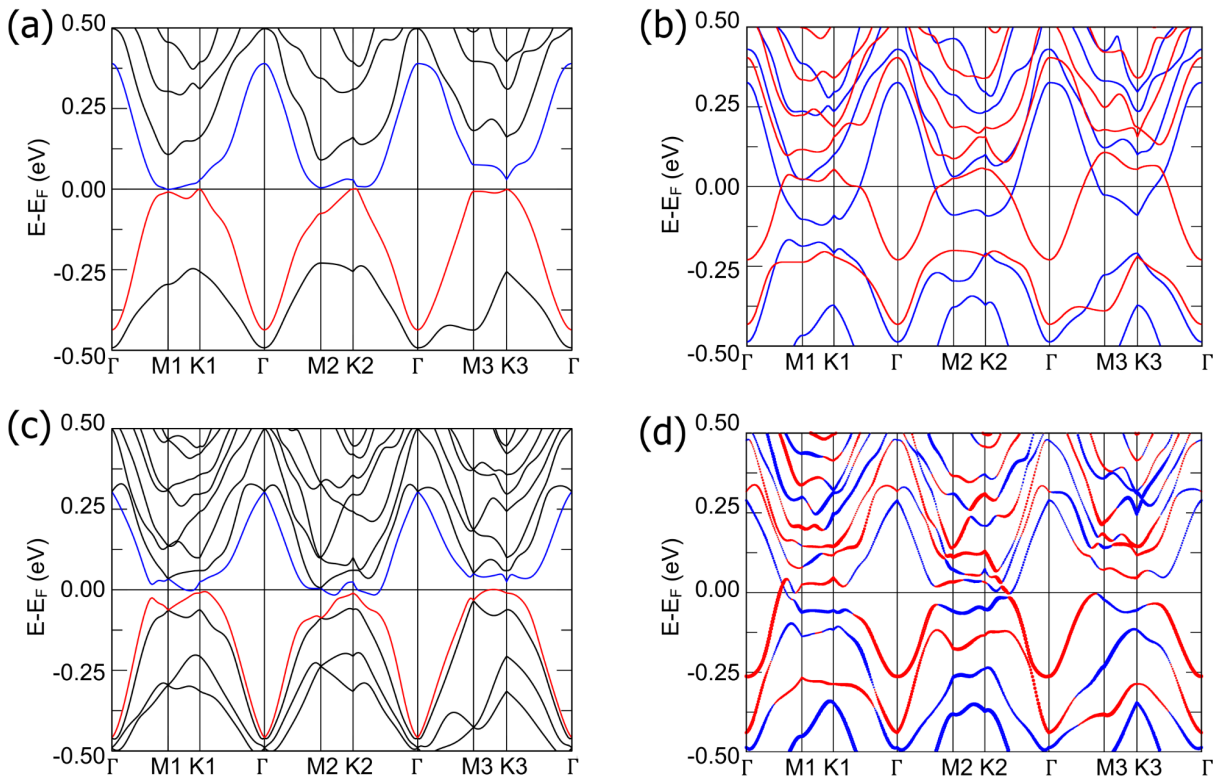

Figure 5. Band structures of hydrogenated $ReSe_2$. The PBE band structures of $1T^{dp}$ 1h-$ReSe_2$ in (a) non-magnetic band calculation without SOC, (b) non-magnetic band calculation with SOC, (c) ferromagnetic band calculation without SOC, and (d) ferromagnetic band calculation with SOC.

4. Conclusions

Through a systematic study based on first-principles calculations, we explored the stability, electronic, thermoelectric, magnetic, and topological properties of Re-based TMDs. With regards to structural stability, the $1T^{dp}$, 1T', 1T, and 2H phases for the pristine bulk and monolayer ReX_2 were considered. Formation energy and phonon dispersion calculations revealed that bulk and monolayer ReX_2 are only stable in the $1T^{dp}$ structure. Van Hove singularities (vHss) are observed among the three monolayers of ReX_2 suggesting possible superconductivity. Regarding the thermoelectric properties, the calculated ZT numbers for the bulk and monolayer $ReTe_2$ at 1300K are 2.10 and 2.30, respectively, which are comparable values to the currently synthesized high-performance thermoelectric materials. In addition, the effect of one- (1h) and two-sided (2h) hydrogenation on the structural, electronic, magnetic, and topological properties of monolayer ReX_2 was also investigated. Upon two-sided hydrogenation, a stable structural phase transition from $1T^{dp}$ to 1T occurred. A ferromagnetic phase transition was also observed upon the two-sided hydrogenation of ReS_2 (2h-ReS_2) and the one-sided hydrogenation of $ReSe_2$ (1h-$ReSe_2$). Finally, one-sided hydrogenation of monolayer $ReSe_2$ and $ReTe_2$ (1h-$ReSe_2$ and 1h-$ReTe_2$) resulted in the non-trivial topological phase transition as confirmed by the calculated Z_2 and Chern topological invariant numbers. Our results show that the ReX_2 monolayers possess highly tunable exotic properties which have excellent potential for thermoelectric and spintronics applications.

Declaration of Competing Interest

The authors declare that they have no known competing financial interests or personal relationships that could have appeared to influence the work reported in this paper.

Author Contributions

F.-C.C. conceived and initiated the study. I.M.R.V. and R.A.B.V. conducted the calculations. All the authors performed the detailed analysis and contributed to discussions and wrote and reviewed the manuscript

Acknowledgments

FCC acknowledges support from the National Center for Theoretical Sciences and the Ministry of Science and Technology of Taiwan under Grant No. MOST-110-2112-M-110-013-MY3. He is also grateful to the National Center for High-performance Computing for the computer time and facilities. HL acknowledges support from the Ministry of Science and Technology of Taiwan under Grant No. MOST 109-2112-M-001-014-MY3.

Supplementary Materials

The supplementary material for this article is available in the online version.

Reference

[1] P. A. Owusu and S. Asumadu-Sarkodie, “A review of renewable energy sources, sustainability issues and climate change mitigation,” *Cogent Engineering*, vol. 3, no. 1, p. 1167990, Dec. 2016, doi: 10.1080/23311916.2016.1167990.

[2] X. Zhang and L.-D. Zhao, “Thermoelectric materials: Energy conversion between heat and electricity,” *Journal of Materiomics*, vol. 1, no. 2, pp. 92–105, Jun. 2015, doi: 10.1016/j.jmat.2015.01.001.

[3] G. J. Snyder and A. H. Snyder, “Figure of merit ZT of a thermoelectric device defined from materials properties,” *Energy Environ. Sci.*, vol. 10, no. 11, pp. 2280–2283, Nov. 2017, doi: 10.1039/C7EE02007D.

[4] P. Mishra, D. Singh, Y. Sonvane, and R. Ahuja, “Two-dimensional boron monochalcogenide monolayer for thermoelectric material,” *Sustainable Energy Fuels*, vol. 4, no. 5, pp. 2363–2369, 2020, doi: 10.1039/D0SE00004C.

[5] A. Patel, D. Singh, Y. Sonvane, P. B. Thakor, and R. Ahuja, “Bulk and monolayer As2S3 as promising thermoelectric material with high conversion performance,” *Computational Materials Science*, vol. 183, p. 109913, Oct. 2020, doi: 10.1016/j.commatsci.2020.109913.

[6] N. Xu, Y. Xu, and J. Zhu, “Topological insulators for thermoelectrics,” *npj Quant Mater*, vol. 2, no. 1, Art. no. 1, Sep. 2017, doi: 10.1038/s41535-017-0054-3.

[7] J. Wu, Y. Chen, J. Wu, and K. Hippalgaonkar, “Perspectives on Thermoelectricity in Layered and 2D Materials,” *Advanced Electronic Materials*, vol. 4, no. 12, p. 1800248, 2018, doi: 10.1002/aelm.201800248.

[8] G. Zhang and Y.-W. Zhang, “Thermoelectric properties of two-dimensional transition metal dichalcogenides,” *J. Mater. Chem. C*, vol. 5, no. 31, pp. 7684–7698, Aug. 2017, doi: 10.1039/C7TC01088E.

[9] D. Li *et al.*, “Recent Progress of Two-Dimensional Thermoelectric Materials,” *Nano-Micro Lett.*, vol. 12, no. 1, p. 36, Jan. 2020, doi: 10.1007/s40820-020-0374-x.

[10] M.-K. Lin *et al.*, “Dimensionality-Mediated Semimetal-Semiconductor Transition in Ultrathin PtTe 2 Films,” *Phys. Rev. Lett.*, vol. 124, no. 3, p. 036402, Jan. 2020, doi: 10.1103/PhysRevLett.124.036402.

[11] R. A. B. Villaos *et al.*, “Thickness dependent electronic properties of Pt dichalcogenides,” *npj 2D Mater Appl*, vol. 3, no. 1, p. 2, Dec. 2019, doi: 10.1038/s41699-018-0085-z.

[12] H. Leng, J.-C. Orain, A. Amato, Y. K. Huang, and A. de Visser, “Type-I superconductivity in the Dirac semimetal PdTe 2 probed by μ SR,” *Phys. Rev. B*, vol. 100, no. 22, p. 224501, Dec. 2019, doi: 10.1103/PhysRevB.100.224501.

[13] R.-S. Chen, C.-C. Tang, W.-C. Shen, and Y.-S. Huang, “Thickness-dependent electrical conductivities and ohmic contacts in transition metal dichalcogenides multilayers,” *Nanotechnology*, vol. 25, no. 41, p. 415706, Oct. 2014, doi: 10.1088/0957-4484/25/41/415706.

[14] H. Zeng and X. Cui, “An optical spectroscopic study on two-dimensional group-VI transition metal dichalcogenides,” *Chem. Soc. Rev.*, vol. 44, no. 9, pp. 2629–2642, 2015, doi: 10.1039/C4CS00265B.

[15] H. N. Cruzado *et al.*, “Band Engineering and Van Hove Singularity on HfX_2 Thin Films (X = S, Se, or Te),” *ACS Appl. Electron. Mater.*, vol. 3, no. 3, pp. 1071–1079, Mar. 2021, doi: 10.1021/acsaelm.0c00907.

[16] R. A. B. Villaos *et al.*, "Evolution of the Electronic Properties of ZrX_2 (X = S, Se, or Te) Thin Films under Varying Thickness," *J. Phys. Chem. C*, vol. 125, no. 1, pp. 1134–1142, Jan. 2021, doi: 10.1021/acs.jpcc.0c10085.
[17] A. B. Maghirang *et al.*, "Predicting two-dimensional topological phases in Janus materials by substitutional doping in transition metal dichalcogenide monolayers," *npj 2D Mater Appl*, vol. 3, no. 1, p. 35, Dec. 2019, doi: 10.1038/s41699-019-0118-2.
[18] L.-Y. Feng *et al.*, "Magnetic and topological properties in hydrogenated transition metal dichalcogenide monolayers," *Chinese Journal of Physics*, vol. 66, pp. 15–23, Aug. 2020, doi: 10.1016/j.cjph.2020.03.018.
[19] J. A. Hlevyack *et al.*, "Dimensional crossover and band topology evolution in ultrathin semimetallic NiTe2 films," *npj 2D Mater Appl*, vol. 5, no. 1, Art. no. 1, Apr. 2021, doi: 10.1038/s41699-021-00218-z.
[20] L.-Y. Feng, R. A. B. Villaos, Z.-Q. Huang, C.-H. Hsu, and F.-C. Chuang, "Layer-dependent band engineering of Pd dichalcogenides: a first-principles study," *New J. Phys.*, vol. 22, no. 5, p. 053010, May 2020, doi: 10.1088/1367-2630/ab7d7a.
[21] M. Z. Hasan, G. Chang, I. Belopolski, G. Bian, S.-Y. Xu, and J.-X. Yin, "Weyl, Dirac and high-fold chiral fermions in topological quantum matter," *Nat Rev Mater*, vol. 6, no. 9, Art. no. 9, Sep. 2021, doi: 10.1038/s41578-021-00301-3.
[22] K.-X. Chen, X.-M. Wang, D.-C. Mo, and S.-S. Lyu, "Thermoelectric Properties of Transition Metal Dichalcogenides: From Monolayers to Nanotubes," *J. Phys. Chem. C*, vol. 119, no. 47, pp. 26706–26711, Nov. 2015, doi: 10.1021/acs.jpcc.5b06728.
[23] A. Patel, D. Singh, Y. Sonvane, P. B. Thakor, and R. Ahuja, "High Thermoelectric Performance in Two-Dimensional Janus Monolayer Material WS-X (X = Se and Te)," *ACS Appl. Mater. Interfaces*, vol. 12, no. 41, pp. 46212–46219, Oct. 2020, doi: 10.1021/acsami.0c13960.
[24] W. Purwitasari *et al.*, "High Thermoelectric Performance in 2D Technetium Dichalcogenides TcX2 (X = S, Se, or Te)," *ACS Appl. Energy Mater.*, Jun. 2022, doi: 10.1021/acsaem.2c01170.
[25] S. Tongay *et al.*, "Monolayer behaviour in bulk ReS2 due to electronic and vibrational decoupling," *Nat Commun*, vol. 5, no. 1, p. 3252, May 2014, doi: 10.1038/ncomms4252.
[26] S. Yang *et al.*, "Layer-dependent electrical and optoelectronic responses of ReSe2 nanosheet transistors," *Nanoscale*, vol. 6, no. 13, p. 7226, 2014, doi: 10.1039/c4nr01741b.
[27] D. Wolverson, S. Crampin, A. S. Kazemi, A. Ilie, and S. J. Bending, "Raman Spectra of Monolayer, Few-Layer, and Bulk $ReSe_2$: An Anisotropic Layered Semiconductor," *ACS Nano*, vol. 8, no. 11, pp. 11154–11164, Nov. 2014, doi: 10.1021/nn5053926.
[28] H.-X. Zhong, S. Gao, J.-J. Shi, and L. Yang, "Quasiparticle band gaps, excitonic effects, and anisotropic optical properties of the monolayer distorted 1T diamond-chain structures ReS2 and ReSe2," *PHYSICAL REVIEW B*, p. 7, 2015.
[29] S. Horzum *et al.*, "Formation and stability of point defects in monolayer rhenium disulfide," *Phys. Rev. B*, vol. 89, no. 15, p. 155433, Apr. 2014, doi: 10.1103/PhysRevB.89.155433.
[30] D. B. Seley, M. Nath, and B. A. Parkinson, "ReSe2 nanotubes synthesized from sacrificial templates," *J. Mater. Chem.*, vol. 19, no. 11, p. 1532, 2009, doi: 10.1039/b809187k.
[31] K. Friemelt, M. ‐Ch. Lux‐Steiner, and E. Bucher, "Optical properties of the layered transition‐metal‐dichalcogenide ReS_2: Anisotropy in the van der Waals plane," *Journal of Applied Physics*, vol. 74, no. 8, pp. 5266–5268, Oct. 1993, doi: 10.1063/1.354268.

[32] C. P. Crisostomo *et al.*, “Robust Large Gap Two-Dimensional Topological Insulators in Hydrogenated III–V Buckled Honeycombs,” *Nano Lett.*, vol. 15, no. 10, pp. 6568–6574, Oct. 2015, doi: 10.1021/acs.nanolett.5b02293.
[33] B.-H. Chou *et al.*, “Hydrogenated ultra-thin tin films predicted as two-dimensional topological insulators,” *New J. Phys.*, vol. 16, no. 11, p. 115008, Nov. 2014, doi: 10.1088/1367-2630/16/11/115008.
[34] C. Zhang and S. Yan, “First-Principles Study of Ferromagnetism in Two-Dimensional Silicene with Hydrogenation,” *J. Phys. Chem. C*, vol. 116, no. 6, pp. 4163–4166, Feb. 2012, doi: 10.1021/jp2104177.
[35] D. C. Elias *et al.*, “Control of Graphene’s Properties by Reversible Hydrogenation: Evidence for Graphane,” *Science*, vol. 323, no. 5914, pp. 610–613, Jan. 2009, doi: 10.1126/science.1167130.
[36] Y. Qu, H. Pan, and C. T. Kwok, “Hydrogenation-controlled phase transition on two-dimensional transition metal dichalcogenides and their unique physical and catalytic properties,” *Sci Rep*, vol. 6, no. 1, p. 34186, Sep. 2016, doi: 10.1038/srep34186.
[37] M. Yagmurcukardes, C. Bacaksiz, R. T. Senger, and H. Sahin, “Hydrogen-induced structural transition in single layer ReS_2,” *2D Mater.*, vol. 4, no. 3, p. 035013, Jul. 2017, doi: 10.1088/2053-1583/aa78c8.
[38] A. Bansil, H. Lin, and T. Das, “Colloquium: Topological band theory,” *Rev. Mod. Phys.*, vol. 88, no. 2, p. 021004, Jun. 2016, doi: 10.1103/RevModPhys.88.021004.
[39] X.-L. Qi and S.-C. Zhang, “Topological insulators and superconductors,” *Rev. Mod. Phys.*, vol. 83, no. 4, pp. 1057–1110, Oct. 2011, doi: 10.1103/RevModPhys.83.1057.
[40] M. Z. Hasan and C. L. Kane, “Colloquium: Topological insulators,” *Rev. Mod. Phys.*, vol. 82, no. 4, pp. 3045–3067, Nov. 2010, doi: 10.1103/RevModPhys.82.3045.
[41] N. Nagaosa, J. Sinova, S. Onoda, A. H. MacDonald, and N. P. Ong, “Anomalous Hall effect,” *Rev. Mod. Phys.*, vol. 82, no. 2, pp. 1539–1592, May 2010, doi: 10.1103/RevModPhys.82.1539.
[42] H. Weng, R. Yu, X. Hu, X. Dai, and Z. Fang, “Quantum anomalous Hall effect and related topological electronic states,” *Advances in Physics*, vol. 64, no. 3, pp. 227–282, May 2015, doi: 10.1080/00018732.2015.1068524.
[43] M. N. R. Perez *et al.*, “Quantum spin Hall insulating phase and van Hove singularities in Zintl single-quintuple-layer AM2X2 (A = Ca, Sr, or Ba; M = Zn or Cd; X = Sb or Bi) family,” *Applied Physics Reviews*, vol. 9, no. 1, p. 011410, Jan. 2022, doi: 10.1063/5.0071687.
[44] C. L. Kane and E. J. Mele, “Z2 Topological Order and the Quantum Spin Hall Effect,” *Phys. Rev. Lett.*, vol. 95, no. 14, p. 146802, Sep. 2005, doi: 10.1103/PhysRevLett.95.146802.
[45] X.-L. Qi, T. L. Hughes, and S.-C. Zhang, “Topological field theory of time-reversal invariant insulators,” *Phys. Rev. B*, vol. 78, no. 19, p. 195424, Nov. 2008, doi: 10.1103/PhysRevB.78.195424.
[46] L. Fu, “Topological Crystalline Insulators,” *Phys. Rev. Lett.*, vol. 106, no. 10, p. 106802, Mar. 2011, doi: 10.1103/PhysRevLett.106.106802.
[47] C.-H. Hsu *et al.*, “Two-dimensional Topological Crystalline Insulator Phase in Sb/Bi Planar Honeycomb with Tunable Dirac Gap,” *Sci Rep*, vol. 6, no. 1, Art. no. 1, Jan. 2016, doi: 10.1038/srep18993.
[48] K. v. Klitzing, G. Dorda, and M. Pepper, “New Method for High-Accuracy Determination

of the Fine-Structure Constant Based on Quantized Hall Resistance," *Phys. Rev. Lett.*, vol. 45, no. 6, pp. 494–497, Aug. 1980, doi: 10.1103/PhysRevLett.45.494.
[49] C. W. J. Beenakker and H. van Houten, "Quantum Transport in Semiconductor Nanostructures," in *Solid State Physics*, vol. 44, H. Ehrenreich and D. Turnbull, Eds. Academic Press, 1991, pp. 1–228. doi: 10.1016/S0081-1947(08)60091-0.
[50] S.-P. Chen *et al.*, "Prediction of Quantum Anomalous Hall Insulator in half-fluorinated GaBi Honeycomb," *Sci Rep*, vol. 6, no. 1, p. 31317, Nov. 2016, doi: 10.1038/srep31317.
[51] G. Kresse and J. Furthmüller, "Efficiency of ab-initio total energy calculations for metals and semiconductors using a plane-wave basis set," *Computational Materials Science*, vol. 6, no. 1, pp. 15–50, Jul. 1996, doi: 10.1016/0927-0256(96)00008-0.
[52] G. Kresse and J. Furthmüller, "Efficient iterative schemes for *ab initio* total-energy calculations using a plane-wave basis set," *Phys. Rev. B*, vol. 54, no. 16, pp. 11169–11186, Oct. 1996, doi: 10.1103/PhysRevB.54.11169.
[53] P. Hohenberg and W. Kohn, "Inhomogeneous Electron Gas," *Phys. Rev.*, vol. 136, no. 3B, pp. B864–B871, Nov. 1964, doi: 10.1103/PhysRev.136.B864.
[54] P. E. Blöchl, "Projector augmented-wave method," *Phys. Rev. B*, vol. 50, no. 24, pp. 17953–17979, Dec. 1994, doi: 10.1103/PhysRevB.50.17953.
[55] G. Kresse and D. Joubert, "From ultrasoft pseudopotentials to the projector augmented-wave method," *Phys. Rev. B*, vol. 59, no. 3, pp. 1758–1775, Jan. 1999, doi: 10.1103/PhysRevB.59.1758.
[56] J. P. Perdew, K. Burke, and M. Ernzerhof, "Generalized Gradient Approximation Made Simple," *Phys. Rev. Lett.*, vol. 77, no. 18, pp. 3865–3868, Oct. 1996, doi: 10.1103/PhysRevLett.77.3865.
[57] I. Hamada, "van der Waals density functional made accurate," *Phys. Rev. B*, vol. 89, no. 12, p. 121103, Mar. 2014, doi: 10.1103/PhysRevB.89.121103.
[58] J. Heyd and G. E. Scuseria, "Efficient hybrid density functional calculations in solids: Assessment of the Heyd–Scuseria–Ernzerhof screened Coulomb hybrid functional," *The Journal of Chemical Physics*, vol. 121, no. 3, pp. 1187–1192, Jul. 2004, doi: 10.1063/1.1760074.
[59] J. Heyd, G. E. Scuseria, and M. Ernzerhof, "Hybrid functionals based on a screened Coulomb potential," *The Journal of Chemical Physics*, vol. 118, no. 18, pp. 8207–8215, May 2003, doi: 10.1063/1.1564060.
[60] J. Heyd, G. E. Scuseria, and M. Ernzerhof, "Erratum: 'Hybrid functionals based on a screened Coulomb potential' [J. Chem. Phys. 118, 8207 (2003)]," *The Journal of Chemical Physics*, vol. 124, no. 21, p. 219906, Jun. 2006, doi: 10.1063/1.2204597.
[61] A. Togo and I. Tanaka, "First principles phonon calculations in materials science," *Scripta Materialia*, vol. 108, pp. 1–5, Nov. 2015, doi: 10.1016/j.scriptamat.2015.07.021.
[62] D. Gresch *et al.*, "Z2Pack: Numerical implementation of hybrid Wannier centers for identifying topological materials," *Phys. Rev. B*, vol. 95, no. 7, p. 075146, Feb. 2017, doi: 10.1103/PhysRevB.95.075146.
[63] A. A. Soluyanov and D. Vanderbilt, "Computing topological invariants without inversion symmetry," *Phys. Rev. B*, vol. 83, no. 23, p. 235401, Jun. 2011, doi: 10.1103/PhysRevB.83.235401.
[64] G. K. H. Madsen and D. J. Singh, "BoltzTraP. A code for calculating band-structure dependent quantities," *Computer Physics Communications*, vol. 175, no. 1, pp. 67–71, Jul. 2006, doi: 10.1016/j.cpc.2006.03.007.

[65] G. K. H. Madsen, J. Carrete, and M. J. Verstraete, “BoltzTraP2, a program for interpolating band structures and calculating semi-classical transport coefficients,” *Computer Physics Communications*, vol. 231, pp. 140–145, Oct. 2018, doi: 10.1016/j.cpc.2018.05.010.
[66] D. I. Bilc and P. Ghosez, “Electronic and thermoelectric properties of Fe${}_{2}$VAl: The role of defects and disorder,” *Phys. Rev. B*, vol. 83, no. 20, p. 205204, May 2011, doi: 10.1103/PhysRevB.83.205204.
[67] A. Togo, L. Chaput, and I. Tanaka, “Distributions of phonon lifetimes in Brillouin zones,” *Phys. Rev. B*, vol. 91, no. 9, p. 094306, Mar. 2015, doi: 10.1103/PhysRevB.91.094306.
[68] L. Chaput, “Direct Solution to the Linearized Phonon Boltzmann Equation,” *Phys. Rev. Lett.*, vol. 110, no. 26, p. 265506, Jun. 2013, doi: 10.1103/PhysRevLett.110.265506.
[69] A. N. Ward, “First Principles Theory of the Lattice Thermal Conductivity of Semiconductors,” Boston College, 2009. Accessed: Jun. 25, 2022. [Online]. Available: http://dlib.bc.edu/islandora/object/bc-ir:101422
[70] J. C. Wildervanck and F. Jellinek, “The dichalcogenides of technetium and rhenium,” *Journal of the Less Common Metals*, vol. 24, no. 1, pp. 73–81, May 1971, doi: 10.1016/0022-5088(71)90168-8.
[71] C. A. Sorrell, “Synthesis of Rhenium Ditelluride,” *J American Ceramic Society*, vol. 51, no. 5, pp. 285–286, May 1968, doi: 10.1111/j.1151-2916.1968.tb13859.x.
[72] Q. He *et al.*, “Deeply Exploring Anisotropic Evolution toward Large-Scale Growth of Monolayer ReS_2,” *ACS Appl. Mater. Interfaces*, vol. 12, no. 2, pp. 2862–2870, Jan. 2020, doi: 10.1021/acsami.9b18623.
[73] S. Jiang *et al.*, “Direct synthesis and in situ characterization of monolayer parallelogrammic rhenium diselenide on gold foil,” *Commun Chem*, vol. 1, no. 1, p. 17, Dec. 2018, doi: 10.1038/s42004-018-0010-6.
[74] B. Jariwala *et al.*, “Synthesis and Characterization of ReS2 and ReSe2 Layered Chalcogenide Single Crystals,” *Chem. Mater.*, vol. 28, no. 10, pp. 3352–3359, May 2016, doi: 10.1021/acs.chemmater.6b00364.
[75] J. P. Echeverry and I. C. Gerber, “Theoretical investigations of the anisotropic optical properties of distorted 1 T ReS 2 and ReSe 2 monolayers, bilayers, and in the bulk limit,” *Phys. Rev. B*, vol. 97, no. 7, p. 075123, Feb. 2018, doi: 10.1103/PhysRevB.97.075123.
[76] A. Arora *et al.*, “Highly Anisotropic in-Plane Excitons in Atomically Thin and Bulklike 1 *T* ′-$ReSe_2$,” *Nano Lett.*, vol. 17, no. 5, pp. 3202–3207, May 2017, doi: 10.1021/acs.nanolett.7b00765.
[77] J. E. Hirsch and D. J. Scalapino, “Enhanced Superconductivity in Quasi Two-Dimensional Systems,” *Phys. Rev. Lett.*, vol. 56, no. 25, pp. 2732–2735, Jun. 1986, doi: 10.1103/PhysRevLett.56.2732.
[78] R. Hlubina, S. Sorella, and F. Guinea, “Ferromagnetism in the Two Dimensional $t - t'$ Hubbard Model at the Van Hove Density,” *Phys. Rev. Lett.*, vol. 78, no. 7, pp. 1343–1346, Feb. 1997, doi: 10.1103/PhysRevLett.78.1343.
[79] C. Honerkamp and M. Salmhofer, “Magnetic and Superconducting Instabilities of the Hubbard Model at the Van Hove Filling,” *Phys. Rev. Lett.*, vol. 87, no. 18, p. 187004, Oct. 2001, doi: 10.1103/PhysRevLett.87.187004.
[80] M. Fleck, A. M. Oleś, and L. Hedin, “Magnetic phases near the Van Hove singularity in s - and d -band Hubbard models,” *Phys. Rev. B*, vol. 56, no. 6, pp. 3159–3166, Aug. 1997, doi: 10.1103/PhysRevB.56.3159.
[81] H. Q. Lin and J. E. Hirsch, “Two-dimensional Hubbard model with nearest- and

next-nearest-neighbor hopping," *Phys. Rev. B*, vol. 35, no. 7, pp. 3359–3368, Mar. 1987, doi: 10.1103/PhysRevB.35.3359.
[82] Y. Y. Wu, X. L. Zhu, H. Y. Yang, Z. G. Wang, Y. H. Li, and B. T. Wang, "First principles calculations on the thermoelectric properties of bulk Au_2S with ultra-low lattice thermal conductivity," *Chinese Phys. B*, vol. 29, no. 8, p. 087202, Jul. 2020, doi: 10.1088/1674-1056/ab973c.
[83] F. Khan *et al.*, "Theoretical investigation of electronic structure and thermoelectric properties of MX2 (M=Zr, Hf; X=S, Se) van der Waals heterostructures," *Journal of Physics and Chemistry of Solids*, vol. 126, pp. 304–309, Mar. 2019, doi: 10.1016/j.jpcs.2018.11.021.
[84] M. Wolf, R. Hinterding, and A. Feldhoff, "High Power Factor vs. High zT—A Review of Thermoelectric Materials for High-Temperature Application," *Entropy*, vol. 21, no. 11, Art. no. 11, Nov. 2019, doi: 10.3390/e21111058.
[85] Z. M. Gibbs, H.-S. Kim, H. Wang, and G. J. Snyder, "Band gap estimation from temperature dependent Seebeck measurement—Deviations from the 2e|S|maxTmax relation," *Appl. Phys. Lett.*, vol. 106, no. 2, p. 022112, Jan. 2015, doi: 10.1063/1.4905922.
[86] S. Raimes, "The rigid-band model," *J. Phys. Radium*, vol. 23, no. 10, pp. 639–643, Oct. 1962, doi: 10.1051/jphysrad:019620023010063901.
[87] S. Bhattacharya and G. K. H. Madsen, "High-throughput exploration of alloying as design strategy for thermoelectrics," *Phys. Rev. B*, vol. 92, no. 8, p. 085205, Aug. 2015, doi: 10.1103/PhysRevB.92.085205.
[88] M. Rull-Bravo, A. Moure, J. F. Fernández, and M. Martín-González, "Skutterudites as thermoelectric materials: revisited," *RSC Adv.*, vol. 5, no. 52, pp. 41653–41667, 2015, doi: 10.1039/C5RA03942H.